ACS APPLIED MATERIALS & INTERFACES

Research Article

www.acsami.org

Synthesis of Magnetite–Graphene Oxide-Layered Double Hydroxide Composites and Applications for the Removal of Pb(II) and 2,4-Dichlorophenoxyacetic Acid from Aqueous Solutions

Fengrong Zhang, Yawen Song, Shue Song, Renjie Zhang, and Wanguo Hou*

Key Laboratory of Colloid and Interface Chemistry (Ministry of Education), Environment Research Institute, Shandong University, Jinan 250100, People's Republic of China

Supporting Information

ABSTRACT: Magnetic composites consisting of magnetite (Fe_3O_4), graphene oxide (GO), and Mg_3Al–OH layered double hydroxide (LDH), denoted as MGL composites, with varying GO contents (R_{GO}) were synthesized by a mechano-hydrothermal (MHT) route using Fe_3O_4, $Mg(OH)_2$, and $Al(OH)_3$ as the inorganic starting materials. The application of the synthesized MGLs for removing the heavy-metal Pb(II) and the hydrophobic organic pesticide 2,4-dichlorophenoxy-acetic acid (2,4-D) from aqueous solutions was investigated. Chemical bonding among the GO, Fe_3O_4, and LDH components was observed in the MGLs. The MGL composites showed good water-dispersity, strong magnetic response, and high sorption capacities and removal efficiencies for both Pb(II) and 2,4-D pollutants. The sorption capacities of the MGL for the pollutants significantly increased with an increase in R_{GO}. Increasing pH could increase the removal efficiency for Pb(II) but decrease that for 2,4-D. The MGLs showed more affinity for Pb(II) than for 2,4-D in the competitive sorption. In addition, the MGLs could remain almost constant removal efficiency for the pollutants after reuse over six cycles, indicating their potential use as sorbents in wastewater treatment. Furthermore, a C_s effect was observed in the sorption equilibriums, which could be described using the Langmuir-SCA and Freundlich-SCA isotherms. The removal mechanisms of the MGL for Pb(II) and 2,4-D were discussed. The MHT method provided a simple and environmentally friendly route for synthesizing GO–LDH composite materials.

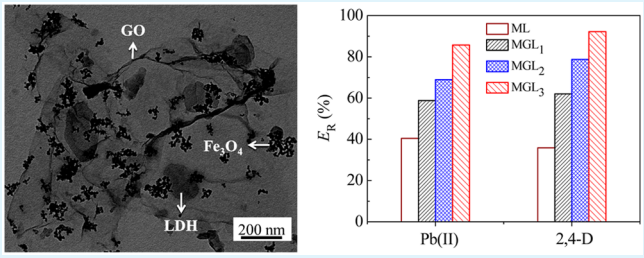

KEYWORDS: *magnetic composite, layered double hydroxide, graphene oxide, sorption, sorbent effect, surface component activity, mechano-hydrothermal method*

1. INTRODUCTION

The increasing worldwide contamination of fresh water systems is one of the key environmental problems facing humanity. Among the thousands of industrial pollutants, the removal of heavy-metal ions and organic pesticides from aqueous solutions has attracted much attention.[1,2] This is because these pollutants can cause severe health problems for both animals and human beings. For example, Pb(II) is a common heavy-metal pollutant arising from both natural and anthropogenic sources. Long-term consumption of Pb(II) will cause serious health disorders such as anemia, cancer, kidney disease, and mental retardation.[3,4] An example of an organic pesticide, 2,4-dichlorophenoxyacetic acid (2,4-D), which is an aromatic compound, has been used as a herbicide on a large scale to control broad-leaved weeds in wheat, rice, and maize, and in aquaculture, resulting in the contamination of both surface and ground waters.[5] Human and animal exposure to 2,4-D can cause serious toxic symptoms.[6] According to the World Health Organization (WHO), the concentrations of Pb(II)[7] and 2,4-D[8] in drinking water should be lower than 10 and 20 μg/L, respectively. Therefore, the removal of heavy-metal[7,9−21] and organic pesticide[8,22−27] pollutants has become a hot topic in environmental science and technology.

Sorption is a widely used technology for the removal of both inorganic and organic pollutants from aqueous solutions because of its simplicity of design, convenience, low cost, high efficiency, and wide adaptability.[18] Many sorbents such as activated carbon, zeolites, minerals (clays), biopolymers, and agro-based and industrial wastes have been tested for removing pollutants from aqueous solutions.[20,21,27] However, such sorbents are associated with certain problems that limit their practical applications, such as low sorption capacity and the difficult separation of the sorbents.[18] Therefore, there is an urgent need to develop new sorbents with higher efficiency and reusability.

Recently, layered double hydroxides (LDHs)[5,9,10,15,16,19] and graphene oxide (GO)[4,7,13,14,16−19,28] have been widely studied as potential sorbents. LDHs, which are also known as

Received: January 15, 2015
Accepted: March 20, 2015
Published: March 20, 2015

DOI: 10.1021/acsami.5b00433
ACS Appl. Mater. Interfaces 2015, 7, 7251−7263

hydrotalcite-like compounds (HTlc) or anionic clays, are a class of lamellar inorganic materials that can be described using the general formula $[M^{II}_{1-x}M^{III}_{x}(OH)_2]^{x+}[(A^{n-})_{x/n}]^{x-}\cdot mH_2O$, where M^{II} and M^{III} are di- and trivalent metal cations, respectively, A^{n-} is the interlayer anion (or gallery anion) of charge n, x is the molar ratio of $M^{III}/(M^{II} + M^{III})$, and m is the molar amount of cointercalated water. The features of LDHs, including their high structural positive charge density, ion-exchange ability, and unique layered nanostructure, result in their high sorption capacity for many pollutants.[10,16] Graphene oxide (GO) and reduced graphene oxide (RGO) are flexible lamellar materials with large specific surface areas and aromatic sp^2 domains. GO possesses a wide range of functional groups such as epoxy (C−O−C), hydroxyl (OH), and carboxyl (COOH) groups on its basal planes and edges.[29] These features impart GO and RGO with excellent sorption capacity for both heavy-metal[4,7,13,14,30−32] and aromatic[33,34] pollutants. Reports concerning the sorption of pollutants on LDHs,[10,35−37] GO,[4,7,30,32] and RGO[31] have been published. However, these materials are used as nanosized sorbent particles and have the disadvantage of difficult separation from liquid phases, which restricts their practical application.[16] To overcome this, magnetite (Fe_3O_4)−LDHs[37] and magnetite−GO (or RGO)[13,14,18,34] composites have been developed and used to remove pollutants from aqueous solutions. These magnetic sorbents can be easily separated from aqueous solutions using magnetic separation. Although LDHs are inexpensive, they have low sorption capability, whereas GO and RGO have efficient sorption capability but are expensive. In view of the requirements for a low-cost, high-efficiency, and reusable sorbent, construction of magnetite−GO (or RGO)−LDH composites for treating wastewater is an excellent choice.[16,19] Wu et al.[16] fabricated magnetite−RGO−LDH composites, and found that they displayed enhanced sorption capacity for As(V) when compared with pure LDHs. However, to the best of our knowledge, there have been no other reports concerning these novel composite sorbents. In addition, in previous studies,[13,16,18,19,34] all the GO (or RGO)−inorganic composites were synthesized by coprecipitation or hydrothermal routes using the corresponding metal salts as inorganic starting materials; these conventional routes have the disadvantage of producing wastewater. Recently, we developed a mechano-hydrothermal (MHT) method to synthesize LDHs using the corresponding metal oxides or hydroxides as starting materials;[38,39] this route does not produce waste, and is therefore environmentally friendly. It is of interest to investigate whether the MHT method can be used to synthesize GO (or RGO)−inorganic composites.

Here, we synthesized composites of magnetite, GO, and Mg_3Al−OH LDH, denoted as MGL composites, by the MHT route using Fe_3O_4, $Mg(OH)_2$, and $Al(OH)_3$ as the inorganic starting materials. Although the magnetite−RGO−LDH composite and the MHT method have been developed, respectively, the synthesis of MGL composites has not yet been reported, especially using the MHT method. The main objectives of this study were to evaluate the technical feasibility of using the MHT method to synthesize MGL composites, and to investigate the application of the synthesized MGL composites for the removal of Pb(II) and 2,4-D from aqueous solutions. Emphasis was placed on the effects of the GO content in the composites and the sorbent dosage used in the removal tests on the sorption capacity of Pb(II) and 2,4-D. To the best of our knowledge, this is the first report on the synthesis of magnetic composites of GO and LDHs and their application for the removal of both heavy-metal and hydrophobic organic pollutants.

2. EXPERIMENTAL SECTION

2.1. Materials. GO (Institute of Coal Chemistry, Chinese Academy of Sciences, China), $Mg(OH)_2$ (Tianjin Damao Chemical Reagent Factory, China), $Al(OH)_3$ (Shanghai Meixing Chemical Co., Ltd., China), $Pb(NO_3)_2$ (Sinopharm Chemical Reagent Co., Ltd., China), and 2,4-D (Shanghai Shisi Hewei Chemical Co., Ltd., China) were of analytical reagent grade, purchased from their respective suppliers, and used as received. Magnetite (Fe_3O_4) was prepared in our laboratory using a previously reported method.[40] Water was purified with a Hitech-Kflow water purification system (Hitech, China).

2.2. Preparation of MGL Composites. Three MGL composite samples were prepared using an MHT method.[38,39] The Mg/Al molar ratio and the Fe_3O_4 content of these samples were held constant at 3:1 and 4.00 wt %, respectively, but their GO content (R_{GO}) varied, being 1.10, 4.13, and 7.92 wt %, which were denoted as MGL_1, MGL_2, and MGL_3, respectively.

A two-step procedure was used to synthesize the target samples. In a typical procedure, a mixture of 17.4 g (0.30 mol) of $Mg(OH)_2$ and 7.80 g (0.10 mol) of $Al(OH)_3$ was milled for 1 h under ambient conditions, using a planetary ball mill (QM3STC, Nanjing Nanda Instrument Plant, China) with four stainless-steel mill pots (500 mL inner volume each), and 10 mm diameter steel balls. The mill speed was 450 rpm with a ball/mixture weight ratio of approximately 49. After that, the milled mixture (1.45 g) was placed in a 100 mL Teflon-lined stainless-steel autoclave filled with 80 mL of an aqueous suspension containing 0.16 g of GO and 0.10 g of Fe_3O_4; the GO and Fe_3O_4 suspensions were previously prepared by dispersing GO and Fe_3O_4 in water using ultrasonication. After the vessel was sealed and shaken thoroughly, it was hydrothermally treated at 100 °C for 24 h in an oven under static conditions. The resulting dispersion was centrifuged and the solid precipitate was washed with water and dried at 60 °C, yielding the MGL_3 sample.

For comparison, a composite of magnetite and Mg_3Al−OH LDH (denoted as ML) was prepared under the same conditions, but in the absence of GO. A reference sample of Mg_3Al−OH LDH was prepared in the same way, but in the absence of both GO and Fe_3O_4.

2.3. Characterization. X-ray diffraction (XRD, D/max-rA, Bruker AXS, Co., Ltd., Germany) patterns of the samples were recorded using Cu Kα radiation (λ = 1.5418 Å) at 40 kV and 40 mA in the 2θ range of 10−70° at a scanning rate of 10°/min. The sample morphology was analyzed using scanning electron microscopy (SEM, JSM-6700F, JEOL, Japan) and transmission electron microscopy (TEM, JEM-2100, JEOL, Japan). The samples for TEM were dispersed in ethanol and then deposited onto amorphous carbon-coated copper grids, and dried before examination. The elemental composition of the samples was determined using inductively coupled plasma-atomic emission spectrometry (ICP-AES, ICAP-9000, Jarrel-ASH, Thermo Electron Co., USA) using samples that were dissolved in dilute HCl, and using elemental analysis (Vario EI III cube V2.0.1, Bruker AXS, Co., Ltd., Germany). Fourier transform infrared spectroscopy (FT-IR, Vector-22, Bruker AXS, Co., Ltd., Germany) of the samples was performed using KBr pellets in reflectance mode, from 400−4000 cm^{-1}, with a resolution of 2 cm^{-1}. Thermogravimetric analysis and differential scanning calorimetry (TGA-DSC, SDT-Q-600, TA Instruments Co., Germany) were performed from ambient temperature to 600 °C at 10 °C/min in a N_2 atmosphere. Magnetic curves were drawn at ambient temperature using vibrating sample magnetometry (VSM, JDM-13, Jilin University, China) in a magnetic field range of 0−13 000 Oe. The N_2 adsorption−desorption isotherms (Autosorb IQ-MP system, Quantachrome Instruments, USA) were determined using samples that were degassed at 120 °C for 5 h under vacuum before measurement. The specific surface area (A_s) and pore volume (V_p) of the samples were calculated from the isotherms using the Brunauer−Emmett−Teller (BET) and Barrett−Joyner−Halenda

DOI: 10.1021/acsami.5b00433
ACS Appl. Mater. Interfaces 2015, 7, 7251−7263

(BJH) methods, respectively. X-ray photoelectron spectroscopy (XPS, Phi 5300 ESCA, PerkinElmer, USA) measurements were performed using the Mg Kα (1253.6 eV) radiation of a twin anode (operated at 200 W) in a constant energy analyzer mode with a pass energy of 30 eV. All of the binding energies were referenced with respect to the C 1s peak (284.8 eV) of the adventitious carbon on the surface.

2.4. Sorption Experiments. The sorption experiments were performed using a batch equilibration technique at 25.0 °C. Pb(II) solutions of various concentrations (0−550 mg/L) were prepared by dissolving $Pb(NO_3)_2$ in water containing 0.010 M of $NaNO_3$. $NaNO_3$ was sued to maintain constant ionic strength of the solutions. 2,4-D solutions of various concentrations (0−3.0 mM) were prepared by dissolving 2,4-D in 10 vol % aqueous ethanol solution containing 0.010 M $NaNO_3$. The ethanol was used to increase the solubility of 2,4-D. The pH values of the Pb(II) and 2,4-D solutions were adjusted to 5.0 and 7.0, respectively, using 0.1 M HNO_3 and NaOH solutions. Known masses of the sorbent samples were mixed with 25 mL of the pollutant solutions in polyethylene centrifuge tubes. The centrifuge tubes were shaken in a thermostatic water bath shaker (Jiangsu Medical Instrument Factory, China) at 25.0 ± 0.2 °C for 24 h. The suspensions were then filtered through a 0.45 μm membrane. The remaining pollutant concentrations in the filtrates were measured using flame atomic absorption spectrometry (TAS-990, Beijing Purkinje General Instrument Co., Ltd., China) for Pb(II), and UV−vis spectrometry (SP-4100, Shanghai Spectrum Instruments Co., Ltd., China) at 282 nm for 2,4-D. The equilibrium sorption amount (Γ_e) and the removal efficiency (E_R) were calculated from the difference between the initial and remaining (or equilibrium) concentrations (C_0 and C_e).

In addition, the sorption amounts (Γ_t) at different sorption times (t), the effect of solution pH on Γ_e, and the competitive sorption of Pb(II) and 2,4-D on the MGLs from their mixed solution were determined, respectively, using the same method.

Recycle tests were also carried out to evaluate the recyclability of the MGLs. After sorption testing, the sorbent particles were collected using a magnet; the Pb(II)-sorbed and 2,4-D-sorbed sorbent particles were thoroughly washed with pH = 4.0 HCl solution and ethanol, respectively, and vacuum-dried at 60 °C for 12 h. The recovered sorbent particles were used for subsequent sorption tests. Six cycles were performed to assess the reusability of the sorbents.

The sorption tests were performed in triplicate and the final values were presented as an average of measurements, with a relative error of less than 4.5%.

3. RESULTS AND DISCUSSION

3.1. Characterization of MGL Composites. Figure 1 shows the XRD patterns of the composite samples, Fe_3O_4, and GO. The Fe_3O_4 and GO exhibited their characteristic diffraction peaks.[13,16,19,41] The ML and MGL samples showed the characteristic diffraction peaks of the LDH-phase (JCPDS No. 51-1528);[42] their d_{003} and d_{006} values were 0.76 and 0.38 nm, respectively, which are consistent with the reported values for Mg−Al−OH LDHs.[42] These XRD results indicated that the LDH-phase had formed in the ML and MGL samples. However, the characteristic diffractions of Fe_3O_4 and GO were indistinct in the XRD patterns of the composite samples because of their low content and the superposition of the diffraction peaks between the two substrates and the LDH-phase. Notably, with increasing R_{GO} (Figure 1 a−d), the 003 peak intensity of the composites increased, which can be attributed to the contribution of the strong 002 basal diffraction of GO. Our XRD data are in good agreement with those reported.[16,42]

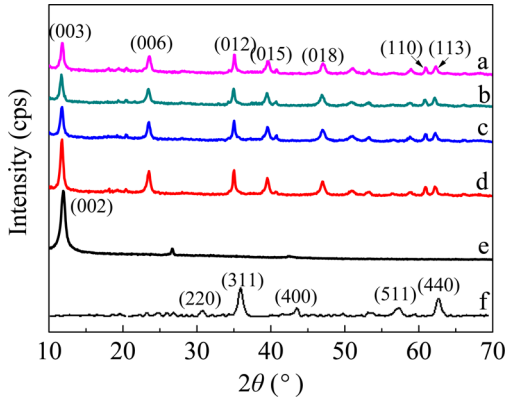

Figure 1. XRD patterns of (a) ML, (b) MGL_1, (c) MGL_2, (d) MGL_3, (e) GO, and (f) Fe_3O_4.

Notably, the synthetic route developed here for MGL composites does not produce any waste, because the water used in the process can be recycled. The recyclability of the water used for producing MGL composites was investigated over six cycles, with no significant change in the XRD patterns of the products. Therefore, this MHT method is a simple and environmentally friendly route for synthesizing organic−LDH composite materials.

Figure 2 shows the SEM and TEM images of the MGL_3 sample; similar images were obtained for the MGL_1 and MGL_2 samples. The MGL sample featured irregular flaky particles (Figure 2A). The Fe_3O_4 sample was composed of spherical particles with a diameter of approximately 20 nm, and the GO sample was composed of wrinkled sheets (Figure S1 in the Supporting Information); each could be distinguished in the MGL sample (Figure 2B, and Figure S1 in the Supporting Information). In addition, hexagonal crystals, typical of LDHs, were observed, and the lateral size of the LDH crystals was ~200 nm. Furthermore, both the Fe_3O_4 nanospheres and LDH crystals appeared to be anchored to the surface of GO (Figure 2B). These SEM and TEM results are similar to those reported.[16]

The elemental analysis data (Table S1 in the Supporting Information) showed that the mole ratio of Mg/Al and the Fe_3O_4 content in all the composites were 2.90−3.14 and 3.88−4.02 wt %, respectively, and the GO contents of MGL_1, MGL_2, and MGL_3 were 0.96, 3.99, and 7.82 wt %, respectively. The chemical compositions of the composite samples were consistent with the mass ratios of the starting materials used in the experiments. Notably, carbon was detected in the ML sample, which indicated the existence of intercalated CO_3^{2-} that arose from CO_2 sorption from the atmosphere.[42]

The N_2 adsorption−desorption isotherms of the ML and MGL samples (Figure S2 in the Supporting Information) exhibited H3 hysteresis loops at P/P_0 ratios higher than ~0.4,[43] which is characteristic of the slit pores arising from the stacking of flaky particles. The A_s, V_p, and average pore size (D_p) of the ML and MGL samples are shown in Table 1. When R_{GO} increased, A_s also increased significantly, whereas V_p and D_p remained almost constant. The high A_s values of the MGL samples are favorable for their application as sorbents.[13,16,34]

Figure 3 shows the FT-IR spectra of MGL_3, Fe_3O_4, GO, and LDH. In the spectrum of Fe_3O_4, the bands at 3421 and 1620 cm^{-1} were attributed to the hydroxyl group and water deformations, and the band at 582 cm^{-1} arose from the stretching vibration of Fe—O.[44] In the spectrum of GO,[41] broad bands at ~3594 and 3421 cm^{-1} were attributed to the O—H stretching vibration of the carboxylic acids and phenolic groups of GO, the strong band at 1727 cm^{-1} was assigned to

DOI: 10.1021/acsami.5b00433
ACS Appl. Mater. Interfaces 2015, 7, 7251−7263

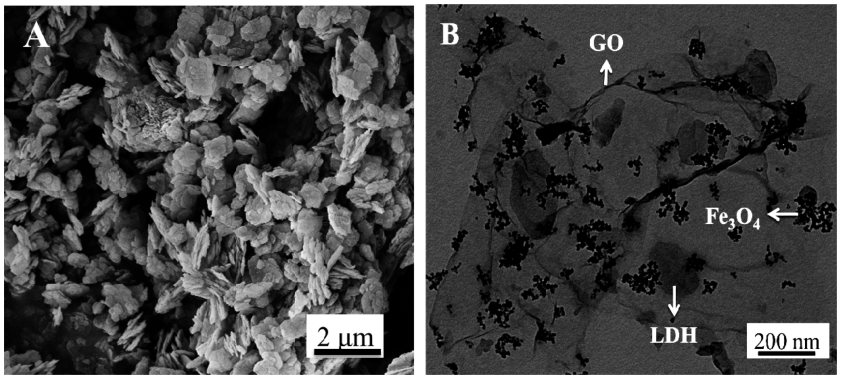

Figure 2. (A) SEM and (B) TEM images of MGL_3.

Table 1. Specific Surface Area and Pore Data of ML and MGL Samples

sample	A_s (m^2/g)	D_p (nm)	V_p (cm^3/g)
ML	36.4	3.83	0.321
MGL_1	41.6	3.83	0.302
MGL_2	51.8	3.83	0.301
MGL_3	74.9	3.84	0.440

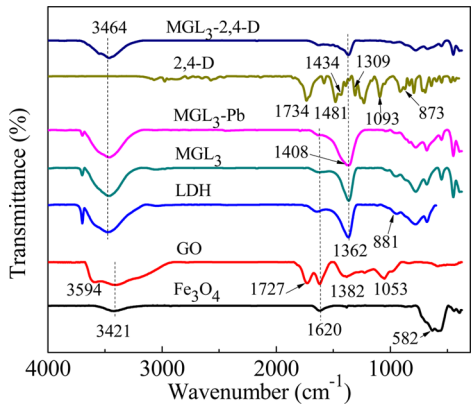

Figure 3. FT-IR spectra of Fe_3O_4, GO, LDH, MGL_3, MGL_3-Pb, 2,4-D, and MGL_3-2,4-D.

the stretching vibration of carbonyl (C═O) groups, another strong band at 1620 cm^{-1} was assigned to the δ_{H-O-H} bending mode, the band at approximately 1382 cm^{-1} arose from the C—OH stretching vibration of the carboxylic acid groups, and the band at 1053 cm^{-1} was attributed to the C—O bending mode. In the spectrum of the LDH sample, the strong broad band centered at approximately 3464 cm^{-1} was assigned to the O—H stretching modes of the hydroxyl groups in the LDH layers and in the interlayer water, and another band corresponding to water deformation was recorded at approximately 1620 cm^{-1}; the bands at 1362 and 881 cm^{-1} were attributed to the ν_3 and ν_2 vibrations of CO_3^{2-}, respectively, indicating the presence of CO_3^{2-} in the LDH-phase;[42] the other peaks from ∼1000 to 400 cm^{-1} were attributed to the stretching and bending of the Mg—O and Al—O lattice.[16] The FT-IR spectrum of the MGL_3 sample presented the same bands as LDH, but the characteristic bands of Fe_3O_4 and GO were not observed clearly because of the superposition of the peaks between the two substrates and the LDH-phase. Notably, the disappearance of the strong bands at 1727 and 1053 cm^{-1} from the GO in the spectrum of the MGL_3 sample possibly arises from the chemical binding of GO with the LDH-phase and Fe_3O_4.

Figure 4 shows the TG-DSC curves of GO, ML, and MGL_3. The weight loss processes of the samples can be divided into

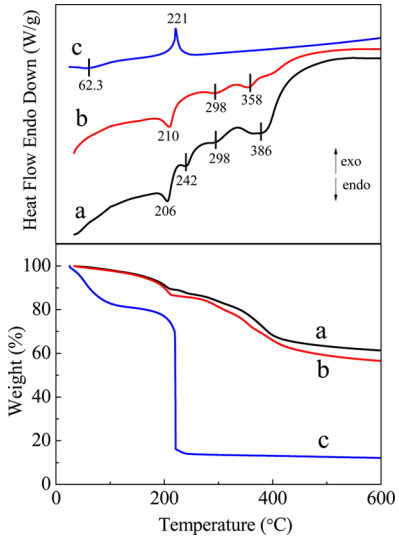

Figure 4. TG-DSC curves of (a) ML, (b) MGL_3, and (c) GO.

two steps. For the GO (Figure 4c), the first weight loss (∼19 wt %) in the 25−150 °C region, with an endothermic peak at ∼62 °C, was attributed to the release of physisorbed water and a slight decomposition of some oxygen-containing groups; the second weight loss (∼67 wt %) in the 150−250 °C region, with an exothermic peak at 221 °C, arose from the major decomposition of oxygen-containing groups.[45,46] For the ML (Figure 4a), the first weight loss (∼13 wt %) in the 25−250 °C region, with two endothermic peaks at 206 and 242 °C, was attributed to the loss of physisorbed and interlayer water and the intercalated OH^-; the second weight loss (∼27 wt %) in the 250−600 °C region, with two endothermic peaks at 298 and 386 °C, arose from the dehydroxylation of brucite-like layers and the decomposition of the intercalated CO_3^{2-} anions.[47] For the MGL_3 (Figure 4b), the first weight loss (∼14 wt %) in the 25−250 °C region, with an endothermic peak at 210 °C, could be attributed to the loss of physisorbed water and the decomposition of the oxygen-containing groups of the GO component; the second weight loss (∼30 wt %) in the 250−600 °C region, with two endothermic peaks at 298 and 358 °C, arose from the decomposition of the LDH-phase.

DOI: 10.1021/acsami.5b00433
ACS Appl. Mater. Interfaces 2015, 7, 7251−7263

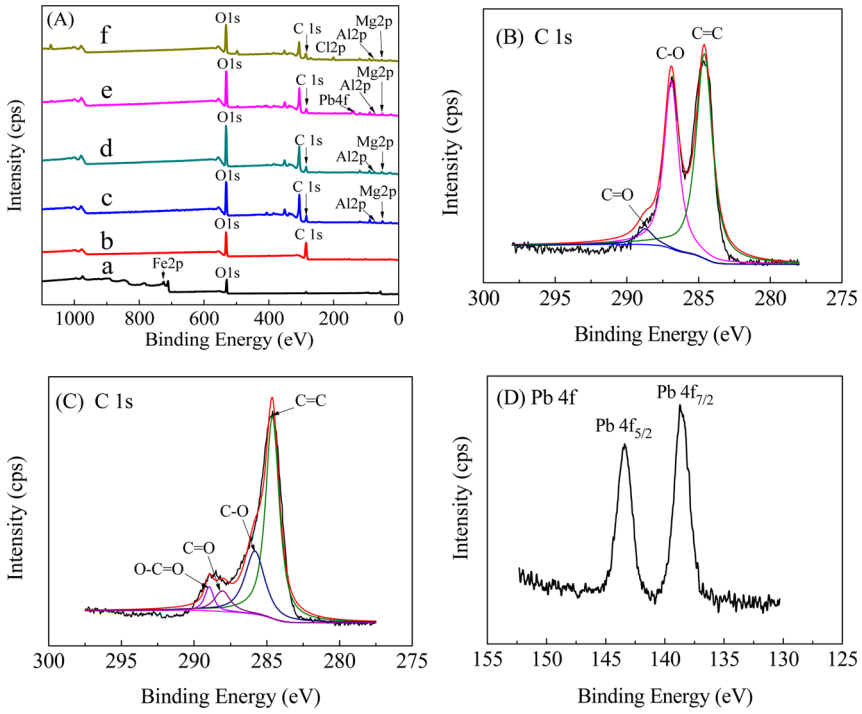

Figure 5. (A) Survey XPS spectra of (a) Fe_3O_4, (b) GO, (c) LDH, (d) MGL_3, (e) MGL_3-Pb, and (f) MGL_3-2,4-D; HR-XPS spectra of C 1s for (B) GO and (C) MGL_3; (D) HR-XPS spectrum of Pb 4f in MGL_3-Pb.

From these TG data, we calculated the R_{GO} in the MGL_3 to be ~8.7 wt %, which is close to that used in the experiment (~7.92 wt %).

To investigate the binding interactions among Fe_3O_4, GO, and LDH in the composites, the XPS spectra of MGL_3, Fe_3O_4, GO, and LDH were analyzed (Figure 5A), and the binding energies (E_B) data for the elements of the samples are summarized in Table 2. Compared to the precursors LDH, GO, and Fe_3O_4, the composite of the three substrates showed a reduction in the E_B value of the C 1s peak by 0.6 eV, and an increase in the E_B values of the Al 2p, Mg 2p, and Fe 2p peaks by 0.8, 1.4, and ~2.7 eV, respectively. The obvious change in the E_B values of these elements before and after the formation of composites suggested that the LDH and Fe_3O_4 particles were chemically bonded to the GO surfaces in the MGL composites. In addition, the high-resolution XPS (HR-XPS) spectrum of C 1s for GO (Figure 5B) indicated that the carbon existed mainly in three forms,[13,48] namely, nonoxygenated carbon (C═C, 284.6 eV), the carbon in C—O (286.9 eV), and the carbonyl carbon (C═O, 288.7 eV); the carboxylate carbon (O—C═O), another form of carbon, was not determined due to its low content. The HR-XPS spectrum of C 1s for the MGL_3 (Figure 5C) presented the peaks of the four forms of carbon, and the C 1s E_B values of the nonoxygenated C, C—O, C═O, and O—C═O peaks were 284.5, 285.9, 288.0, and 288.9 eV, respectively (Table S2 in the Supporting Information). Compared to the GO, the E_B values of C 1s of the C—O and C═O forms in the MGL_3 decreased by 1.0 and 0.7 eV, respectively, whereas that of the nonoxygenated C had no obvious change; this indicated that the LDH and Fe_3O_4 were chemically bonded to the oxygenated functional groups on the GO surface.

Table 2. Binding Energies of Elements in LDH, GO, Fe_3O_4, MGL_3, MGL_3-Pb, and MGL_3-2,4-D

	E_B (eV)				
sample	C 1s	O 1s	Al 2p	Mg 2p	Fe 2p
LDH		531.6	74.40	50.00	
GO	285.4	532.4			
Fe_3O_4		530.2			724.1
MGL_3	284.8	531.9	75.20	51.40	726.8
MGL_3-Pb	284.6	531.8	74.80	50.50	
MGL_3-2,4-D	285.2	532.0	75.70	52.10	

The magnetization curves of the Fe_3O_4 and MGL_3 samples were measured at ambient temperature (Figure S3 in the Supporting Information). The results indicated that both Fe_3O_4 and MGL_3 were superparamagnetic. The specific saturation magnetizations (M_s) of the Fe_3O_4 and MGL_3 samples were 27.3 and 3.5 emu/g, respectively. The reduction in the M_s value for the MGL_3 compared to that for Fe_3O_4 is a consequence of presence of the nonmagnetic LDH and GO in the composite. However, even such a low M_s value for the MGL_3 was sufficient for its magnetic response to an external magnetic field, as indicated by the following magnetic separation tests (Figure 6). The black MGL_3 particles were dispersed in water in a glass vial by hand-shaking, which produced a stable black homodispersion. This revealed that the MGL_3 sample showed good water-dispersity. The black particles were quickly attracted toward a magnet placed near the glass vial, and the solution became colorless and transparent within ~5 min, which demonstrated the strong magnetic sensitivity of the magnetic composite. Thus, the MGL composites can be easily separated using a magnetic separation process after being used for the removal of pollutants from aqueous solutions. However, when a physical mixture of the LDH and Fe_3O_4, or that of the LDH, Fe_3O_4, and GO, was used instead of the MGL_3 composite in the same magnetic separation tests, no colorless and transparent solutions were obtained after ~1 h (Figure S4 in the

DOI: 10.1021/acsami.5b00433
ACS Appl. Mater. Interfaces 2015, 7, 7251−7263

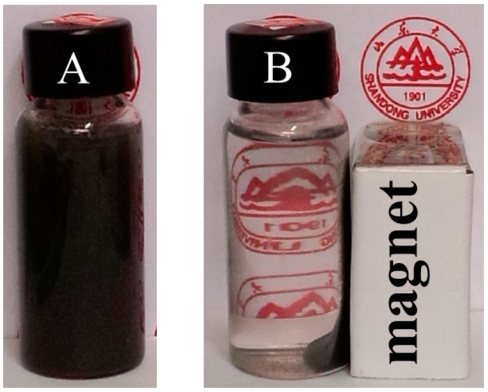

Figure 6. Photographs of MGL_3 aqueous dispersion (A) before and (B) after magnetic separation for 5 min.

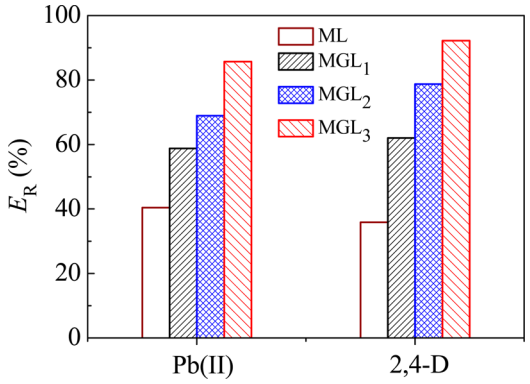

Figure 7. Removal efficiency of ML and MGL for Pb(II) (C_0 = 30 mg/L, pH = 5.0) and 2,4-D (C_0 = 0.01 mM, pH = 7.0). C_s = 1.0 g/L, 25 °C, and C_{NaNO_3} = 0.010 M.

Supporting Information). These results also confirmed that there were chemical bonding interactions among the GO, Fe_3O_4, and LDH components in the MGL composites.

We concluded that the MGL composites were successfully synthesized by the MHT method using the corresponding metal oxides as inorganic starting materials. Chemical bonds were formed among the GO, Fe_3O_4, and LDH components during the hydrothermal treatment. As suggested by Wu et al.,[16] during the hydrothermal process, the LDH plates might have grown directly on the GO surface, and both the Fe_3O_4 nanoparticles and LDH plates were covalently anchored to the GO through its surface functional groups.

3.2. Removal Performance of MGL Composites for Pb(II) and 2,4-D. *3.2.1. Removal Efficiency and Sorption Isotherm.* Sorption kinetic tests of the MGL_3 for Pb(II) (C_0 = 300 mg/L, pH = 5.0) and 2,4-D (C_0 = 3.0 mM, pH = 7.0) were first performed to evaluate the contact time needed for sorption equilibrium, where the sorbent dosage (C_s) was 1.0 g/L, the concentration of $NaNO_3$ (C_{NaNO_3}) was 0.010 M, and the temperature was 25 °C. The results showed that the sorption amount significantly increased within the first 2 h, followed by a slow increase until equilibrium was reached (Figure S5 in the Supporting Information). The necessary time to reach equilibrium was about 10 h. A contact time of 24 h was chosen to determine Γ_e to ensure sorption equilibrium. In addition, we found that the sorption kinetic processes could be described by the pseudo-second-order kinetic model (Figure S5 in the Supporting Information). Similar results were reported for GO (or RGO)-based sorbents.[13,16,18,19]

The removal efficiencies of the ML and MGL composites for Pb(II) (C_0 = 30 mg/L, pH = 5.0) and 2,4-D (C_0 = 0.01 mM, pH = 7.0) from aqueous solutions were determined at C_s = 1.0 g/L, C_{NaNO_3} = 0.010 M, and 25 °C, as shown in Figure 7. The E_R values of the MGL composites were obviously higher than that of the ML composite. Furthermore, the E_R of the MGL composites increased with an increase in R_{GO}, which indicated that the compositing of GO with LDHs could significantly improve the removal performance of the LDHs for both heavy-metal and aromatic pollutants from aqueous solutions. The maximum E_R values of the MGL_3 were high at 87.2% for Pb(II) and 92.5% for 2,4-D under the studied conditions. Furthermore, the E_R values of the MGL_3 for Pb(II) and 2,4-D at extremely low concentrations, C_0 = 0.25 mg/L for Pb(II) and C_0 = 0.0025 mM (or 0.55 mg/L) for 2,4-D, were determined under the same conditions, being 96.8% and 97.5%, respectively; the residual concentrations of Pb(II) and 2,4-D after sorption were ~8 and 14 μg/L, respectively, which are lower than the WHO drinking water quality standard levels (10 μg/L for Pb(II) and 20 μg/L for 2,4-D).[7,8] These results indicate the potential of the MGL composites as the sorbents for wastewater and drinking water treatments.

To evaluate the recyclability of the sorbents, recycle tests were performed using MGL_3 at C_s = 1.0 g/L, C_{NaNO_3} = 0.010 M, and 25 °C, where C_0 = 30 mg/L and pH = 5.0 for Pb(II), and C_0 = 0.01 mM and pH = 7.0 for 2,4-D. Desorption efficiencies (E_D) of sorbed Pb(II) and 2,4-D from MGL_3 were first determined.[7] It was found that the E_D values of the sorbed Pb(II) in pH = 4.0 HCl solution and the sorbed 2,4-D in ethanol were ~94.8% and 97.8%, respectively. The pH = 4.0 HCl solution and ethanol as eluents were thus used for the recycle tests. Six cycles were performed, and the E_R values for Pb(II) and 2,4-D were found to be declined only by less than 9% and 8%, respectively (Figure S6 in the Supporting Information). The morphological stability of the recovered MGL_3 was examined using SEM, and no significant change in its morphology was observed over six cycles (Figure S6 in the Supporting Information). These results indicate that the MGL composites have a good recyclability for removing both heavy-metal and hydrophobic organic pollutants from wastewater.

To evaluate the uptake capability of the ML and MGL composites for Pb(II) and 2,4-D, the sorption isotherms were measured at C_s = 1 g/L, C_{NaNO_3} = 0.010 M, pH = 5.0 for Pb(II) and 7.0 for 2,4-D, and 25 °C, as shown in Figure 8. All the isotherms were L-type, indicating that the composites have high affinity for Pb(II) and 2,4-D.

Sorption isotherms are commonly described using the Langmuir or Freundlich isotherms. The Langmuir model can be expressed in a nonlinear form as

$$\Gamma_e = \frac{K_L \Gamma_m C_e}{1 + K_L C_e} \quad (1)$$

or in a linear form as

$$\frac{C_e}{\Gamma_e} = \frac{C_e}{\Gamma_m} + \frac{1}{K_L \Gamma_m} \quad (2)$$

The Freundlich model can be expressed in a nonlinear form as

$$\Gamma_e = K_F C_e^{n_F} \quad (3)$$

or in a linear form as

DOI: 10.1021/acsami.5b00433
ACS Appl. Mater. Interfaces 2015, 7, 7251−7263

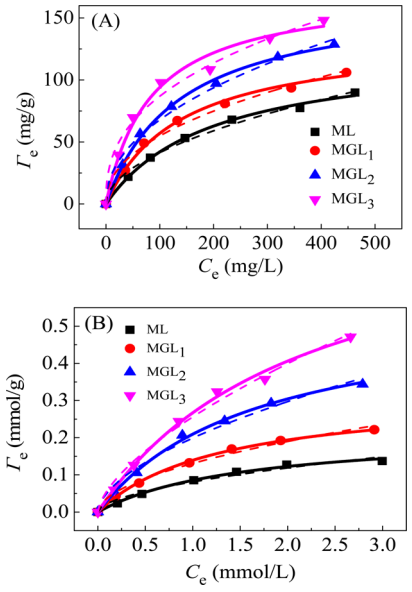

Figure 8. Sorption isotherms of (A) Pb(II) and (B) 2,4-D on ML and MGL. C_s = 1.0 g/L, C_{NaNO_3} = 0.010 M, 25 °C, pH 5.0 for Pb(II) and pH 7.0 for 2,4-D. The dots represent experimental data, the solid lines represent Langmuir model fits, and the dashed lines represent Freundlich model fits.

$$\lg \Gamma_e = \lg K_F + n_F \lg C_e \quad (4)$$

In these equations, Γ_m is the maximum sorption amount, K_L is the Langmuir equilibrium constant, and K_F and n_F are the Freundlich constants.

The sorption data for the various composites were fitted using the Langmuir and Freundlich isotherms using nonlinear and linear regressions. All of the nonlinear model plots coincided with the experimental data (Figure 8), and the linear model plots were straight lines (Figure S7 in the Supporting Information). The best-fit values of the model parameters, Γ_m, K_L, K_F, n_F, and the correlation coefficient (R^2), are listed in Tables 3 and 4 (and Tables S3 and S4 in the Supporting Information). High correlation (R^2) values were obtained for the various model-fitting plots, indicating that both the Langmuir and Freundlich models adequately described the sorption isotherms for the various composites. In addition, the best-fit values of the model parameters using nonlinear and linear regressions were very similar. Furthermore, it can be seen from Tables 3 and 4 that the Γ_m values in mg/g obviously increased with increasing R_{GO}. This can be attributed to the increase in the A_s of the composites induced by the introduction of GO[16] and the high sorption capability of GO for the pollutants.[4,18,30,32−34]

By considering the maximum sorption amount per unit area (Γ_m values in mg/m^2 for Pb(II) and mmol/m^2 for 2,4-D) for the various composites, we obtained more information about contribution of each component in the removal of Pb(II) and 2,4-D. In Tables 3 and 4, the Γ_m values in mg/m^2 for Pb(II) were similar for the ML and the various MGL composites, whereas those in mmol/m^2 for 2,4-D increased with increasing R_{GO}. This indicated that effect of the GO for the enhancement of Pb(II) sorption arose from the increase in the A_s of the composites induced by GO, whereas that for the sorption of 2,4-D arose from the strong sorption of the GO component for the pollutant in particular. Using the R_{GO} and Γ_m data for the ML and MGL composites, the sorption capability of the GO component for 2,4-D was calculated to be ~8.6 mmol/g, which is much higher than that of the ML (0.219 mmol/g). These results suggested that the removal of Pb(II) was mainly a consequence of the sorption contribution from the LDH component, whereas the removal of 2,4-D arose from the sorption contributions from both the LDH and GO components. This was proven by the XPS data (see section 3.2.4).

The pH of solution is one of the most important parameters affecting sorption process. The effects of pH on the uptake capabilities of the MGL_3 for Pb(II) (C_0 = 30 and 100 mg/L) and 2,4-D (C_0 = 0.15 and 0.25 mM) were investigated at C_s = 1.0 g/L, C_{NaNO_3} = 0.010 M, and 25 °C. With increasing pH from 4−10, the Γ_e and E_R for Pb(II) increased while those for 2,4-D decreased, as shown in Figure 9 (and Figure S8 in the Supporting Information). Similar results were reported in the literature.[8,13,18,19,25−27] The pK_a (K_a, acid dissociation constant) of 2,4-D is about pH ~2.8,[5,49,50] and the isoelectric point of the MGL_3 was determined at C_{NaNO_3} = 0.010 M to be pH ~3.5 (Figure S9 in the Supporting Information). Therefore, both the MGL_3 and 2,4-D were negatively charged in the studied pH range (4−10). The results of pH affecting the sorption can be explained with the electrostatic interaction between the MGL_3 and the pollutants. Increasing pH can enhance the electrostatic attraction of the MGL_3 for Pb(II) but the electrostatic repulsion of the MGL_3 for 2,4-D, thus resulting in an increase in the Γ_e and E_R for Pb(II) but a decrease in those for 2,4-D. In addition, the removal of Pb(II) at high pH value (above 8.5) can be attributed to the precipitation of Pb(II) hydroxides.[7,18]

The sorption selectivity of the MGL_3 for Pb(II) and 2,4-D was also determined from their mixed solution containing 95 mg/L Pb(II) and 0.20 mM 2,4-D, where pH = 5.0, C_s = 1.0 g/L, C_{NaNO_3} = 0.010 M, and 25 °C. The results showed that the Γ_e and E_R for Pb(II) from the mixed Pb(II)/2,4-D solution were 61.3 mg/g and 64.5%, and those for 2,4-D were 0.089 mmol/g and 44.7%, respectively. Under the same conditions, the Γ_e and E_R for Pb(II) from the monocomponent 95 mg/L Pb(II) solution were determined to be 63.6 mg/g and 67.0%, and those for 2,4-D from the monocomponent 0.20 mM 2,4-D solution were determined to be 0.169 mmol/g and 84.7%, respectively. Compared with the sorption data for Pb(II) and 2,4-D from the monocomponent solutions, no significant

Table 3. Nonlinear-Fit Data of Model Parameters for Pb(II) Sorption on ML and MGL

	Langmuir isotherm				Freundlich isotherm		
sample	Γ_m (mg/g)	mg/m^2	$K_L \times 10^3$ (L/mg)	R^2	K_F (L^{n_F} mg$^{1-n_F}$/g)	n_F	R^2
ML	125	3.42	5.09	0.997	3.92	0.512	0.990
MGL_1	135	3.25	7.29	0.996	6.93	0.449	0.987
MGL_2	168	3.25	7.35	0.998	7.96	0.465	0.990
MGL_3	173	2.31	11.9	0.987	14.5	0.388	0.983

DOI: 10.1021/acsami.5b00433
ACS Appl. Mater. Interfaces 2015, 7, 7251−7263

Table 4. Nonlinear-Fit Data of Model Parameters for 2,4-D Sorption on ML and MGL

	Langmuir isotherm				Freundlich isotherm		
sample	Γ_m mmol/g	Γ_m (mmol/m^2)	K_L (L/mmol)	R^2	K_F (L^{n_F} mg$^{1-n_F}$/g)	n_F	R^2
ML	0.219	6.04×10^{-3}	0.643	0.995	0.081	0.551	0.970
MGL_1	0.321	7.69×10^{-3}	0.775	0.999	0.131	0.537	0.986
MGL_2	0.560	10.8×10^{-3}	0.605	0.998	0.199	0.578	0.981
MGL_3	0.901	12.0×10^{-3}	0.790	0.996	0.375	0.548	0.992

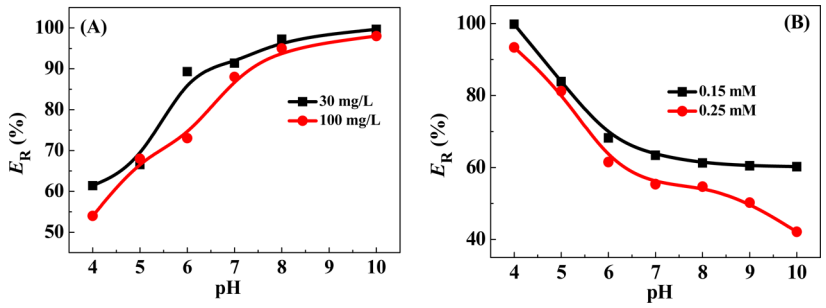

Figure 9. Effects of pH on the removal efficiency of MGL_3 for (A) Pb(II) (C_0 = 30 and 100 mg/L) and (B) 2,4-D (C_0 = 0.15 and 0.25 mM). C_s = 1.0 g/L, C_{NaNO_3} = 0.010 M, and 25 °C.

change in the Γ_e and E_R for Pb(II) but an obvious decrease in those for 2,4-D were observed from the mixed Pb(II)/2,4-D solution. This indicates that the MGL composites have more affinity for Pb(II) than for 2,4-D, which can be explained with the electrostatic interaction between the MGL and the pollutants.

3.2.2. Effect of Sorbent Dosage. The sorbent amounts used in sorption tests are an important factor influencing the sorption capacity of solid sorbents in aqueous solutions.[18,51,52] Studying the effect of the C_s on the sorption is of theoretical and practical significance. Using the MGL_3 as an example, the sorption isotherms for Pb(II) and 2,4-D at different C_s values were measured at C_{NaNO_3} = 0.010 M, pH = 5.0 for Pb(II) and 7.0 for 2,4-D, and 25 °C, as shown in Figure 10. The sorption isotherms significantly declined with increasing C_s. The C_s-dependence of the sorption isotherms is a well-known solid (or sorbent concentration) effect (C_s effect).[51−56]

The sorption data at various C_s values were fitted using the Langmuir and Freundlich isotherms using nonlinear and linear regressions. All of the nonlinear model plots coincided with the experimental data (Figure 10), and the linear model plots were straight lines (Figure S10 in the Supporting Information). The best-fit values of the model parameters, Γ_m, K_L, K_F, n_F, and R^2, are listed in Tables 5 and 6 (and Tables S5 and S6 in the Supporting Information). High R^2 values for the various model-fitting plots indicated that both the Langmuir and Freundlich models adequately described the sorption isotherms for any given C_s value. In addition, the best-fit values of the model parameters using nonlinear and linear regressions were very similar. Furthermore, it can be seen from Tables 5 and 6 that the Γ_m values decreased with increasing C_s. In fact, all of the Langmuir and Freundlich parameters varied with C_s. Similar results were reported in the literature.[55,56] The C_s-dependence of the model parameters violates the predictions of the Langmuir and Freundlich models.

The Langmuir model is based on thermodynamic equilibrium, whereas the Freundlich model is originally an empirical equation. However, Sheindorf et al.[57] revealed that the Freundlich isotherm can be thermodynamically derived based on the assumption that (i) the sorption sites of sorbent have

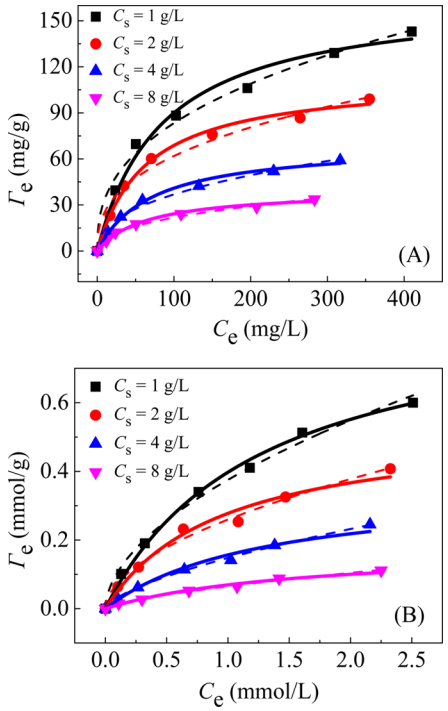

Figure 10. Sorption isotherms of (A) Pb(II) (pH 5.0) and (B) 2,4-D (pH 7.0) on MGL_3 at different sorbent dosages. C_{NaNO_3} = 0.010 M, 25 °C. The dots represent experimental data, the solid lines represent Langmuir model fits, and the dashed lines represent Freundlich model fits.

different energies, and (ii) the sorption of sorbate on the sites having the same energy level obeys the Langmuir isotherm. That is, the Langmuir and Freundlich isotherms are both thermodynamic equilibrium equations. Therefore, as thermodynamic parameters, the K_L, Γ_m, K_F, and n_F should be independent of both the sorbent and sorbate concentrations. The C_s-dependence of these parameters, which was observed in numerous sorption equilibrium studies,[51−56] cannot be described or predicted by either of the two models. This is

DOI: 10.1021/acsami.5b00433
ACS Appl. Mater. Interfaces 2015, 7, 7251−7263

Table 5. Nonlinear-Fit Data of Model Parameters for Pb(II) Sorption on MGL_3 at Different C_s Values

	Langmuir isotherm			Freundlich isotherm		
C_s (g/L)	Γ_m mg/g	K_L L/mg	R^2	K_F (L^{n_F} mg^{1-n_F}/g)	n_F	R^2
1.00	173	0.0119	0.987	14.5	0.388	0.983
2.00	113	0.0156	0.994	10.7	0.380	0.980
4.00	69.9	0.0141	0.993	5.30	0.421	0.987
8.00	39.7	0.0156	0.992	3.06	0.426	0.985

Table 6. Nonlinear-Fit Data of Model Parameters for 2,4-D Sorption on MGL_3 at Different C_s Values

	Langmuir isotherm			Freundlich isotherm		
C_s (g/L)	Γ_m mmol/g	K_L (L/mmol)	R^2	K_F (L^{n_F} mg^{1-n_F}/g)	n_F	R^2
1.00	0.901	0.790	0.996	0.375	0.548	0.992
2.00	0.541	1.060	0.983	0.260	0.541	0.987
4.00	0.359	0.769	0.981	0.147	0.653	0.997
8.00	0.181	0.626	0.987	0.065	0.676	0.993

because interactions between solid sorbent particles exist in real systems, whereas the two models do not account for these interactions. As a result, they only describe the sorption equilibrium of ideal systems. In addition, a disadvantage of the C_s-dependence of the parameters is that the values obtained at a given C_s value cannot be used to predict the sorption capacity of the sorbents at other C_s values.

3.2.3. Analysis of the Solid Effect with a Surface Component Activity Model. To describe the C_s-dependence of the sorption capability of a sorbent, we developed a surface component activity (SCA) model,[54−56] where the activity coefficient of the sorption sites on the sorbent surfaces is assumed to be a function of C_s rather than unity, which considers the existence of interactions between the solid particles. Two C_s-dependent thermodynamic sorption equations, the Langmuir-SCA and Freundlich-SCA isotherms, were derived based on the SCA model.[55,56]

The Langmuir-SCA and Freundlich-SCA isotherms can be represented, respectively, as follows

$$\frac{\Gamma_e}{f_s} = \frac{K_{eq}\Gamma_m^0 C_e}{1 + K_{eq}C_e} \quad (5)$$

$$\Gamma_e = K_s f_s C_e^{n_s} \quad (6)$$

or in their linear forms as follows

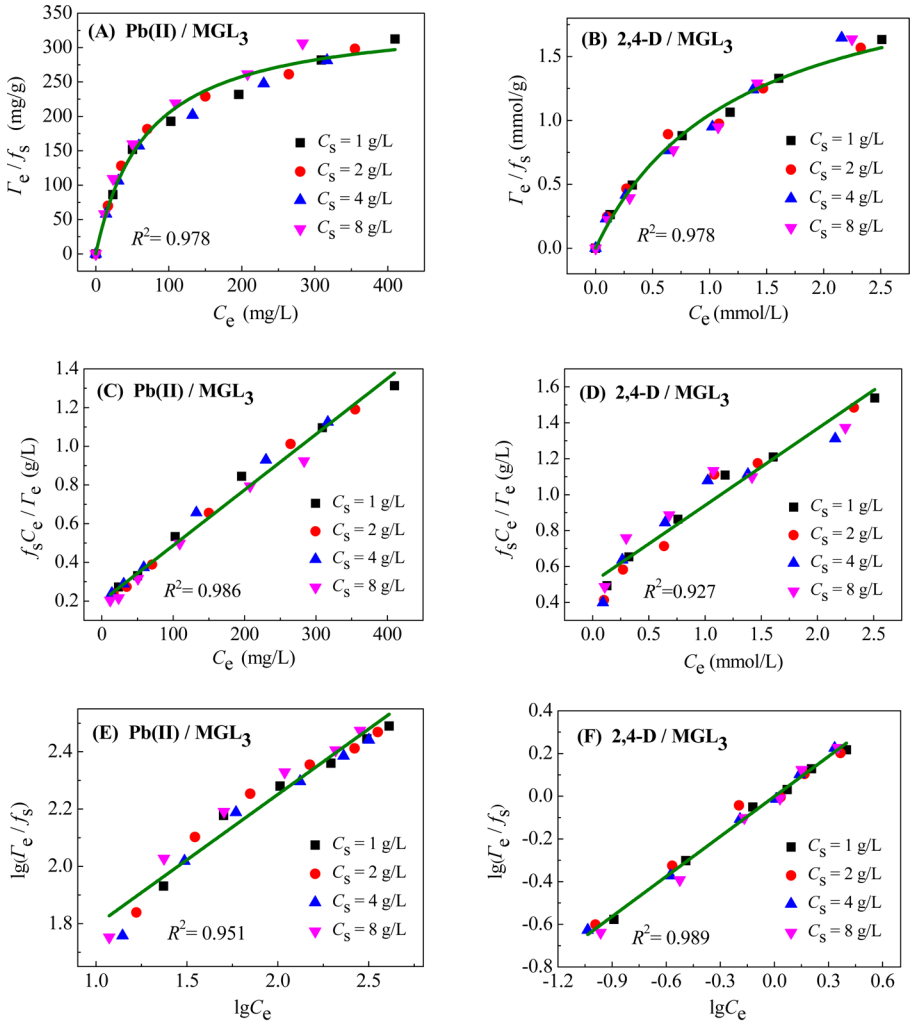

Figure 11. SCA model plots of (A, C, E) Pb(II) and (B, D, F) 2,4-D sorption on MGL_3 at different sorbent dosages.

DOI: 10.1021/acsami.5b00433
ACS Appl. Mater. Interfaces 2015, 7, 7251−7263

$$\frac{f_s C_e}{\Gamma_e} = \frac{C_e}{\Gamma_m^0} + \frac{1}{K_{eq}\Gamma_m^0} \quad (7)$$

$$\lg\left(\frac{\Gamma_e}{f_s}\right) = n_s \lg C_e + \lg K_s \quad (8)$$

In these equations, f_s is the activity coefficient of the sorbent surface sites; K_{eq} is the intrinsic Langmuir equilibrium constant; Γ_m^0 is the characteristic saturation sorption capacity, which corresponds to a saturated monolayer adsorption of the total actual sorption sites; K_s and n_s are the intrinsic Freundlich constants. For a given system at constant temperature, pressure, and medium composition (e.g., pH, ionic strength), the intrinsic parameters, K_{eq}, Γ_m^0, K_s, and n_s, are independent of C_s.

In our previous work,[54−56] an exponential form of the C_s-dependent function of f_s was suggested as follows

$$f_s = \exp(-\gamma C_s^{\alpha}) \quad (9)$$

where γ and α are empirical constants. In addition, the relationships between the intrinsic parameters in the SCA model and the corresponding parameters in the Langmuir and Freundlich isotherms were obtained as follows

$$\Gamma_m = \Gamma_m^0 \exp(-\gamma C_s^{\alpha}) \quad (10)$$

$$K_F = K_s \exp(-\gamma C_s^{\alpha}) \quad (11)$$

The above equations can be used to simulate the empirical constants, γ and α, in f_s from sorption data.

The Γ_m and K_F data at various C_s values were fitted using eqs 10 and 11. We found that the α value could be set to 0.5, because the plots of $\ln\Gamma_m \sim C_s^{0.5}$ and $\ln K_F \sim C_s^{0.5}$ were all fairly straight lines (Figure S11 in Supporting Information). The γ values for Pb(II) and 2,4-D, which were obtained from the slopes of the $\ln\Gamma_m \sim C_s^{0.5}$ and $\ln K_F \sim C_s^{0.5}$ plots, were 0.76 ± 0.02 and 0.91 ± 0.05 $L^{0.5}/g^{0.5}$, respectively.

If the Langmuir-SCA and Freundlich-SCA isotherms are applicable, the plots of f_sC_e/Γ_e vs C_e and $\lg(\Gamma_e/f_s)$ vs $\lg C_e$ should be linear and independent of C_s, and the plot of Γ_e/f_s vs C_e for various C_s should result a unique curve. The sorption data at different C_s values were fitted using the Langmuir-SCA and Freundlich-SCA isotherms, as shown in Figure 11. Indeed, a unique C_s-independent curve of Γ_e/f_s vs C_e, and linear plots for both f_sC_e/Γ_e vs C_e and $\lg(\Gamma_e/f_s)$ vs $\lg C_e$ were obtained, and the R^2 values of these plots were higher than 0.92. These results revealed that both the Langmuir-SCA and Freundlich-SCA models adequately described the sorption equilibriums with the C_s-effect. From the slopes and intercepts of the linear model plots, the intrinsic model parameters, K_{eq}, Γ_m^0, K_s, and n_s, for Pb(II) were calculated to be 0.014 L/mg, 347.2 mg/g, 21.74 L^n_s mg^{1-n}_s/g, and 0.457, respectively; and those for 2,4-D were calculated to be 0.834 L/mmol, 2.34 mmol/g, 0.997 L^n_s $mmol^{1-n}_s$/g, and 0.625, respectively. Because of their C_s-independence, the values of these intrinsic model parameters can be used to predict the sorption capacity of the sorbent at any C_s value. Because the C_s can significantly influence the sorption capacity of sorbents, one should use the Γ_m^0, rather than the Γ_m at a given C_s, to compare the sorption capacities of different sorbents.

Unfortunately, no Γ_m^0 values for sorbents have been reported, therefore the sorption capacities at given C_s values are commonly used to compare the sorption capabilities of different sorbents. Some previously studied sorbents exhibited a sorption capacity for Pb(II) in the range of 21−113 mg/g at C_s = 0.3−10 g/L, pH 5.2−7.0, and 25−30 °C, specific examples include: bentonite (23.8 mg/g at C_s = 0.5 g/L),[11] iron oxide (27.0 mg/g at C_s = 10 g/L),[12] activated carbon (21.8 mg/g at C_s = 6.5 g/L),[58] sawdust (34.3 mg/g at C_s = 5 g/L),[59] hazelnut shell (28.2 mg/g at C_s = 0.4 g/L),[60] LDH−humate hybrid (99.4 mg/g at C_s = 1.7 g/L),[61] and SiO_2/graphene composite (113 mg/g at C_s = 0.3 g/L).[17] In our case, the sorption capacity of the MGL_3 was 39.7−173 mg/g or 0.53−2.31 mg/m^2, at C_s = 8−1 g/L, pH 5.0, and 25 °C. Previous studies[25−27] have revealed that the sorption capacity of activated carbon materials for 2,4-D is approximately 0.19−0.38 mmol/g at C_s = 1 g/L, pH 7, and 25−30 °C. In our case, the sorption capacity of the MGL_3 was 0.90 mmol/g at C_s = 1 g/L, pH 7.0, and 25 °C. These data showed that the sorption capacity of the MGL_3 for both Pb(II) and 2,4-D was obviously higher than that of the previously studied common sorbents. Notably, many novel sorbents with high sorption capacities for Pb(II) have been reported, such as sandwichlike magnesium silicate/RGO nanocomposite (416 mg/g or 0.92 mg/m^2 at C_s = 1 g/L)[62] and magnesium silicate hollow spheres (300 mg/g or 0.58 mg/m^2 at C_s = 0.5 g/L).[63] The sorption capacities in mg/g of these novel sorbents for Pb(II) are higher than that of the MGL_3, but their sorption capacities in mg/m^2 (normalized by A_s) are lower than that of the MGL_3. These results indicate that the MGL composites are promising sorbents for treating wastewater containing heavy-metal and aromatic pollutants.

3.2.4. Discussion on Removal Mechanism. To investigate the removal mechanisms of the MGL composites for Pb(II) and 2,4-D, the MGL_3 samples were characterized by XRD, FT-IR, and XPS techniques after sorbing the pollutants. The Pb(II)-loaded MGL_3 (MGL_3-Pb) sample was prepared at C_0 = 300 mg/L, pH = 5.0, and C_s = 1 g/L, and the 2,4-D-loaded MGL_3 (MGL_3-2,4-D) sample was prepared at C_0 = 0.5 mM, pH = 7.0, and C_s = 1 g/L.

The XRD pattern of the MGL_3-Pb exhibited the characteristic diffraction peaks of hydrocerussite $Pb_3(CO_3)_2(OH)_2$ (Figure S12 in the Supporting Information), indicating that precipitation of $Pb_3(CO_3)_2(OH)_2$ was a Pb(II) sorption mechanism. We previously observed this surface-induced precipitation sorption of Pb(II) on LDHs.[9] In addition, the characteristic diffraction peaks of the LDH-phase disappeared in the MGL_3-Pb sample, which can be attributed to the screening of the $Pb_3(CO_3)_2(OH)_2$ precipitate for the LDH-phase diffractions. In the XRD pattern of the MGL_3-2,4-D sample (Figure S12 in the Supporting Information), the characteristic diffraction peaks of LDH-phase were observed, but their relative intensities had obviously decreased. An additional peak at a low 2θ (~8.21°) was observed, which can be attributed to the intercalation of 2,4-D anions into the gallery of the partial LDH-phase via an anion-exchange process with the interlayer anions OH^- and CO_3^{2-}. Similar results were reported in the literature.[5,64]

The FT-IR spectra of the MGL_3-Pb and MGL_3-2,4-D samples are shown in Figure 3. The spectrum of pristine 2,4-D is also shown in the figure for comparison. In the 2,4-D spectrum, the band at 1734 cm^{-1} was assigned to the stretching vibration of the carbonyl (C═O) group, the bands at 1481 and 1434 cm^{-1} were assigned to aromatic C═C bond vibrations, the bands at 1309 and 1093 cm^{-1} were assigned to the antisymmetric and symmetric vibrations of C—O—C, respectively, and the band at 873 cm^{-1} was assigned to the C—Cl vibration.[64] In the MGL_3-2,4-D sample spectrum, the

DOI: 10.1021/acsami.5b00433
ACS Appl. Mater. Interfaces 2015, 7, 7251−7263

characteristic bands of 2,4-D were not clearly observed due to its low concentration in the sample. However, the intensity of the peak at ~1362 cm^{-1}, which corresponded to CO_3^{2-} in the LDH-phase, significantly decreased when compared with pristine MGL_3, indicating that an anion-exchange between the 2,4-D and CO_3^{2-} anions occurred during the sorption process. The MGL_3-Pb sample spectrum was similar to that of the MGL_3 sample, however a shoulder peak appeared at approximately 1408 cm^{-1}, near the original CO_3^{2-} band at 1362 cm^{-1}, which might be due to the CO_3^{2-} in the $Pb_3(CO_3)_2(OH)_2$ precipitate.[65] In addition, the area of the CO_3^{2-} band at ~1362 cm^{-1} for the MGL_3-Pb increased when compared with pristine MGL_3, which can be attributed to the contribution of CO_3^{2-} from the $Pb_3(CO_3)_2(OH)_2$ precipitate.

The survey XPS spectra of the MGL_3-Pb and MGL_3-2,4-D samples are shown in Figure 5A, and the peaks corresponding to Pb 4f and Cl 2p were clearly observed at E_B ~140 and 200 eV, respectively. The E_B values of the various elements in the samples are listed in Table 2. Notably, the Fe 2p signal in the MGL_3-Pb and MGL_3-2,4-D samples was too weak to determine its E_B value, possibly due to their low Fe content. The loading of Pb(II) in the MGL_3-Pb sample led to a decrease in E_B of Al 2p and Mg 2p by about 0.4 and 0.9 eV, respectively, when compared with pristine MGL_3; however, no obvious change in the E_B of C 1s and O 1s was observed. This indicated that strong interactions occurred between the loaded Pb(II) and the LDH-phase, but no strong interactions occurred between the loaded Pb(II) and the GO component. In addition, in the HR-XPS spectrum of Pb 4f of the MGL_3-Pb sample (Figure 5D), the peaks of Pb $4f_{5/2}$ and $4f_{7/2}$ appeared at E_B 143.5 and 138.5 eV, respectively, which are higher than their E_B values in PbO (141.7 and 136.9 eV), but are consistent with those in the Pb(II)−CO_3^{2-} binding state.[66] This indicated that $Pb_3(CO_3)_2(OH)_2$ formed and that the loaded Pb(II) mainly existed as $Pb_3(CO_3)_2(OH)_2$. In the MGL_3-2,4-D sample spectrum, the loading of 2,4-D led to an increase in the E_B of C 1s by 0.4 eV, a decrease in the E_B of Al 2p and Mg 2p by 0.5 and 0.7 eV, respectively, and no obvious change in the E_B of O 1s, when compared with the pristine MGL_3. This indicated that strong interactions occurred between the loaded 2,4-D and both the GO and LDH components. Furthermore, due to the E_B of O 1s being unchanged by the loading of either Pb(II) or 2,4-D on the MGL_3, it appears that no chemical binding to O between the sorbates and the sorbent occurred.

On the basis of these results, we concluded that there were different removal mechanisms for Pb(II) and 2,4-D by the MGL composites. The removal of Pb(II) mainly arose from the sorption contribution of the LDH component via a process of surface-induced precipitation of $Pb_3(CO_3)_2(OH)_2$. The removal of 2,4-D arose from the sorption contributions of both the LDH and the GO components. The sorption of 2,4-D on the LDH component primarily occurred through the intercalation of 2,4-D anions into the LDH gallery via an anion-exchange process, whereas that on the GO component was attributed to their $\pi-\pi$ and hydrophobic interactions.[67,68] These removal mechanisms are consistent with the Γ_m data in mg/m^2 for various composites (Tables 3 and 4).

4. CONCLUSION

Magnetic composites consisting of Fe_3O_4, GO, and Mg_3Al−OH LDH were successfully synthesized using an MHT route. Chemical bonding occurred among the GO, Fe_3O_4, and LDH components of the MGL composites. The MGL composites exhibited good water-dispersity, strong magnetic response, and high Γ_m and E_R for both Pb(II) and 2,4-D pollutants. Increasing the R_{GO} could increase the A_s of the MGL and enhance their sorption capability for the pollutants. More affinity of the MGLs for Pb(II) than for 2,4-D was observed in the competitive sorption. With increasing pH from 4−10, the E_R for Pb(II) increased but that for 2,4-D decreased. After reuse over 6 cycles, the MGLs could remain almost constant E_R for the pollutants. The sorption of Pb(II) and 2,4-D on the MGLs showed an obvious C_s-effect, which could be described by the Langmuir-SCA and Freundlich-SCA isotherms. Different mechanisms were identified for removing Pb(II) and 2,4-D by the MGLs. The removal of Pb(II) occurred mainly from the sorption contribution of the LDH component via surface-induced precipitation of $Pb_3(CO_3)_2(OH)_2$, whereas that of 2,4-D occurred mainly owing to the sorption contributions of both the LDH and GO components. The sorption of 2,4-D on the LDH component was primarily through the intercalation of 2,4-D anions into the LDH gallery, whereas that on the GO component was attributed to their $\pi-\pi$ and hydrophobic interactions. MGL composites are potential sorbents for wastewater treatment. The MHT method provides a simple and environmentally friendly route for synthesizing GO−LDH composite materials. To the best of our knowledge, this is the first report of the magnetic composites of GO and LDHs and their application for the removal of both heavy-metal and hydrophobic organic pollutants.

■ ASSOCIATED CONTENT

Supporting Information

TEM and SEM images, elemental analysis data, N_2 adsorption−desorption isotherms, XRD patterns, and hysteresis curves of various samples, binding energies of various type C 1s in GO and MGL_3, photographs of aqueous dispersions of the LDH/Fe_3O_4 and LDH/Fe_3O_4/GO physical mixtures, recycle test data of MGL_3 for Pb(II) and 2,4-D, effect of pH on sorption amount and ζ-potential of MGL_3, and fitting plots and best-fit parameter values of kinetic and isotherm models for sorption data. This material is available free of charge via the Internet at http://pubs.acs.org/.

■ AUTHOR INFORMATION

Corresponding Author

*W. Hou. E-mail: wghou@sdu.edu.cn. Tel: +86-0531-88564750. Fax: +86-0531-88564750.

Notes

The authors declare no competing financial interest.

■ ACKNOWLEDGMENTS

This research was supported by the National Natural Science Foundation of China (Nos. 21173135 and 21403128).

■ REFERENCES

(1) Schwarzenbach, R. P.; Escher, B. I.; Fenner, K.; Hofstetter, T. B.; Johnson, C. A.; Von Gunten, U.; Wehrli, B. The Challenge of Micropollutants in Aquatic Systems. *Science* **2006**, *313*, 1072−1077.

(2) Carvalho, M.; Pereira, C.; Goncalves, I.; Pinheiro, H.; Santos, A.; Lopes, A.; Ferra, M. Assessment of the Biodegradability of a Monosulfonated Azo Dye and Aromatic Amines. *Int. Biodeterior. Biodegrad.* **2008**, *62*, 96−103.

(3) Li, Y.-H.; Wang, S.; Wei, J.; Zhang, X.; Xu, C.; Luan, Z.; Wu, D.; Wei, B. Lead Adsorption on Carbon Nanotubes. *Chem. Phys. Lett.* **2002**, *357*, 263−266.

DOI: 10.1021/acsami.5b00433
ACS Appl. Mater. Interfaces 2015, 7, 7251−7263

(4) Zhao, G.; Ren, X.; Gao, X.; Tan, X.; Li, J.; Chen, C.; Huang, Y.; Wang, X. Removal of Pb(II) Ions from Aqueous Solutions on Few-Layered Graphene Oxide Nanosheets. *Dalton Trans.* **2011**, *40*, 10945−10952.
(5) Legrouri, A.; Lakraimi, M.; Barroug, A.; De Roy, A.; Besse, J. P. Removal of the Herbicide 2,4-Dichlorophenoxyacetate from Water to Zinc−Aluminium−Chloride Layered Double Hydroxides. *Water Res.* **2005**, *39*, 3441−3448.
(6) Farah, M. A.; Ateeq, B.; Ali, M. N.; Sabir, R.; Ahmad, W. Studies on Lethal Concentrations and Toxicity Stress of Some Xenobiotics on Aquatic Organisms. *Chemosphere* **2004**, *55*, 257−265.
(7) Madadrang, C. J.; Kim, H. Y.; Gao, G.; Wang, N.; Zhu, J.; Feng, H.; Gorring, M.; Kasner, M. L.; Hou, S. Adsorption Behavior of EDTA-Graphene Oxide for Pb(II) Removal. *ACS Appl. Mater. Interfaces* **2012**, *4*, 1186−1193.
(8) Gupta, V. K.; Suhas, I. Ali; Saini, V. K. Adsorption of 2,4-D and Carbofuran Pesticides Using Fertilizer and Steel Industry Wastes. *J. Colloid Interface Sci.* **2006**, *299*, 556−563.
(9) Liang, X.; Zang, Y.; Xu, Y.; Tan, X.; Hou, W.; Wang, L.; Sun, Y. Sorption of Metal Cations on Layered Double Hydroxides. *Colloids Surf., A* **2013**, *433*, 122−131.
(10) Goh, K.; Lim, T.; Dong, Z. Application of Layered Double Hydroxides for Removal of Oxyanions: A Review. *Water Res.* **2008**, *42*, 1343−1368.
(11) Wang, S.; Dong, Y.; He, M.; Chen, L.; Yu, X. Characterization of GMZ Bentonite and Its Application in the Adsorption of Pb(II) from Aqueous Solutions. *Appl. Clay Sci.* **2009**, *43*, 164−171.
(12) Nassar, N. N. Rapid Removal and Recovery of Pb(II) from Wastewater by Magnetic Nanoadsorbents. *J. Hazard. Mater.* **2010**, *184*, 538−546.
(13) Chandra, V.; Park, J.; Chun, Y.; Lee, J. W.; Hwang, I. C.; Kim, K. S. Water-Dispersible Magnetite-Reduced Graphene Oxide Composites for Arsenic Removal. *ACS Nano* **2010**, *4*, 3979−3986.
(14) Zhu, J.; Wei, S.; Gu, H.; Rapole, S. B.; Wang, Q.; Luo, Z.; Haldolaarachchige, N.; Young, D. P.; Guo, Z. One-Pot Synthesis of Magnetic Graphene Nanocomposites Decorated with Core@Double-shell Nanoparticles for Fast Chromium Removal. *Environ. Sci. Technol.* **2011**, *46*, 977−985.
(15) Gong, J.; Liu, T.; Wang, X.; Hu, X.; Zhang, L. Efficient Removal of Heavy Metal Ions from Aqueous Systems with the Assembly of Anisotropic Layered Double Hydroxide Nanocrystals@Carbon Nanosphere. *Environ. Sci. Technol.* **2011**, *45*, 6181−6187.
(16) Wu, X.-L.; Wang, L.; Chen, C.-L.; Xu, A.-W.; Wang, X.-K. Water-Dispersible Magnetite-Graphene-LDH Composites for Efficient Arsenate Removal. *J. Mater. Chem.* **2011**, *21*, 17353−17359.
(17) Hao, L.; Song, H.; Zhang, L.; Wan, X.; Tang, Y.; Lv, Y. SiO_2/Graphene Composite for Highly Selective Adsorption of Pb(II) Ion. *J. Colloid Interface Sci.* **2012**, *369*, 381−387.
(18) Liu, M.; Chen, C.; Hu, J.; Wu, X.; Wang, X. Synthesis of Magnetite/Graphene Oxide Composite and Application for Cobalt(II) Removal. *J. Phys. Chem. C* **2011**, *115*, 25234−25240.
(19) Wen, T.; Wu, X.; Tan, X.; Wang, X.; Xu, A. One-Pot Synthesis of Water-Swellable Mg−Al Layered Double Hydroxides and Graphene Oxide Nanocomposites for Efficient Removal of As(V) from Aqueous Solutions. *ACS Appl. Mater. Interfaces* **2013**, *5*, 3304−3311.
(20) Miretzky, P.; Cirelli, A. F. Cr(VI) and Cr(III) Removal from Aqueous Solution by Raw and Modified Lignocellulosic Materials: A Review. *J. Hazard. Mater.* **2010**, *180*, 1−19.
(21) Bailey, S. E.; Olin, T. J.; Bricka, R. M.; Adrian, D. D. A Review of Potentially Low-Cost Sorbents for Heavy Metals. *Water Res.* **1999**, *33*, 2469−2479.
(22) McTernan, W. F.; Pereira, J. A. Biotransformation of Lindane and 2,4-D in Batch Enrichment Cultures. *Water Res.* **1991**, *25*, 1417−1423.
(23) Brillas, E.; Calpe, J. C.; Casado, J. Mineralization of 2,4-D by Advanced Electrochemical Oxidation Processes. *Water Res.* **2000**, *34*, 2253−2262.
(24) Kamble, S. P.; Deosarkar, S. P.; Sawant, S. B.; Moulijn, J. A.; Pangarkar, V. G. Photocatalytic Degradation of 2,4-Dichlorophenoxyacetic Acid Using Concentrated Solar Radiation: Batch and Continuous Operation. *Ind. Eng. Chem. Res.* **2004**, *43*, 8178−8187.
(25) Aksu, Z.; Kabasakal, E. Batch Adsorption of 2,4-Dichlorophenoxy-Acetic Acid (2,4-D) from Aqueous Solution by Granular Activated Carbon. *Sep. Purif. Technol.* **2004**, *35*, 223−240.
(26) Aksu, Z.; Kabasakal, E. Adsorption Characteristics of 2,4-Dichlorophenoxyacetic Acid (2,4-D) from Aqueous Solution on Powdered Activated Carbon. *J. Environ. Sci. Health, Part B* **2005**, *40*, 545−570.
(27) Hameed, B. H.; Salman, J. M.; Ahmad, A. L. Adsorption Isotherm and Kinetic Modeling of 2,4-D Pesticide on Activated Carbon Derived from Date Stones. *J. Hazard. Mater.* **2009**, *163*, 121−126.
(28) Lü, K.; Zhao, G.; Wang, X. A Brief Review of Graphene-based Material Synthesis and Its Application in Environmental Pollution Management. *Chin. Sci. Bull.* **2012**, *57*, 1223−1234.
(29) Lerf, A.; He, H.; Forster, M.; Klinowski, J. Structure of Graphite Oxide Revisited. *J. Phys. Chem. B* **1998**, *102*, 4477−4482.
(30) Yang, S.-T.; Chang, Y.; Wang, H.; Liu, G.; Chen, S.; Wang, Y.; Liu, Y.; Cao, A. Folding/Aggregation of Graphene Oxide and Its Application in Cu^{2+} Removal. *J. Colloid Interface Sci.* **2010**, *351*, 122−127.
(31) Koo, H. Y.; Lee, H. J.; Go, H. A.; Lee, Y. B.; Bae, T. S.; Kim, J. K.; Choi, W. S. Graphene-based Multifunctional Iron Oxide Nanosheets with Tunable Properties. *Chem.—Eur. J.* **2011**, *17*, 1214−1219.
(32) Lee, Y. C.; Yang, J. W. Self-Assembled Flower-like TiO_2 on Exfoliated Graphite Oxide for Heavy Metal Removal. *J. Ind. Eng. Chem.* **2012**, *18*, 1178−1185.
(33) Zhao, G.; Jiang, L.; He, Y.; Li, J.; Dong, H.; Wang, X.; Hu, W. Sulfonated Graphene for Persistent Aromatic Pollutant Management. *Adv. Mater.* **2011**, *23*, 3959−3963.
(34) Geng, Z.; Lin, Y.; Yu, X.; Shen, Q.; Ma, L.; Li, Z.; Pan, N.; Wang, X. Highly Efficient Dye Adsorption and Removal: A Functional Hybrid of Reduced Graphene Oxide-Fe_3O_4 Nanoparticles as an Easily Regenerative Adsorbent. *J. Mater. Chem.* **2012**, *22*, 3527−3535.
(35) Baliarsingh, N.; Parida, K. M.; Pradhan, G. C. Influence of the Nature and Concentration of Precursor Metal Ions in the Brucite Layer of LDHs for Phosphate Adsorption - A Review. *RSC Adv.* **2013**, *3*, 23865−23878.
(36) Wang, R.-X.; Wen, T.; Wu, X.-L.; Xu, A.-W. Highly Efficient Removal of Humic Acid from Aqueous Solutions by Mg/Al Layered Double Hydroxides-Fe_3O_4 Nanocomposites. *RSC Adv.* **2014**, *4*, 21802−21809.
(37) Chen, D.; Li, Y.; Zhang, J.; Li, W.; Zhou, J.; Shao, L.; Qian, G. Efficient Removal of Dyes by a Novel Magnetic Fe_3O_4/ZnCr-Layered Double Hydroxide Adsorbent from Heavy Metal Wastewater. *J. Hazard. Mater.* **2012**, *243*, 152−160.
(38) Zhang, F.; Du, N.; Song, S.; Liu, J.; Hou, W. Mechano-Hydrothermal Synthesis of Mg_2Al−NO_3 Layered Double Hydroxides. *J. Solid State Chem.* **2013**, *206*, 45−50.
(39) Zhang, F.; Du, N.; Li, H.; Liu, J.; Hou, W. Synthesis of Mg−Al−Fe−NO_3 Layered Double Hydroxides via a Mechano-Hydrothermal Route. *Solid State Sci.* **2014**, *32*, 41−47.
(40) Kang, Y. S.; Risbud, S.; Rabolt, J. F.; Stroeve, P. Synthesis and Characterization of Nanometer-Size Fe_3O_4 and γ-Fe_2O_3 Particles. *Chem. Mater.* **1996**, *8*, 2209−2211.
(41) Wang, Y.; Zhang, D.; Bao, Q.; Wu, J.; Wan, Y. Controlled Drug Release Characteristics and Enhanced Antibacterial Effect of Graphene Oxide-Drug Intercalated Layered Double Hydroxide Hybrid Films. *J. Mater. Chem.* **2012**, *22*, 23106−23113.
(42) Tongamp, W.; Zhang, Q.; Saito, F. Preparation of Meixnerite (Mg−Al−OH) Type Layered Double Hydroxide by a Mechanochemical Route. *J. Mater. Sci.* **2007**, *42*, 9210−9215.
(43) Hu, W.; Gu, H.; Wang, J.; Li, Y.; Wang, Z. One-Step Synthesis of Silica Hollow Particles in a W/O Inverse Emulsion. *Colloid Polym. Sci.* **2013**, *291*, 2697−2704.
(44) Waldron, R. D. Infrared Spectra of Ferrites. *Phys. Rev.* **1955**, *99*, 1727−1735.

DOI: 10.1021/acsami.5b00433
ACS Appl. Mater. Interfaces 2015, 7, 7251−7263

(45) Zhu, C.; Guo, S.; Fang, Y.; Dong, S. Reducing Sugar: New Functional Molecules for the Green Synthesis of Graphene Nanosheets. *ACS Nano* **2010**, *4*, 2429−2437.
(46) Fang, Q.; Chen, B. Self-Assembly of Graphene Oxide Aerogels by Layered Double Hydroxides Cross-Linking and Their Application in Water Purification. *J. Mater. Chem. A* **2014**, *2*, 8941−8951.
(47) Cavani, F.; Trifirò, F.; Vaccari, A. Hydrotalcite-Type Anionic Clays: Preparation, Properties and Applications. *Catal. Today* **1991**, *11*, 173−301.
(48) Bonanni, A.; Ambrosi, A.; Chua, C. K.; Pumera, M. Oxidation Debris in Graphene Oxide Is Responsible for Its Inherent Electroactivity. *ACS Nano* **2014**, *8*, 4197−4204.
(49) Wauchope, R. D.; Buttler, T. M.; Hornsby, A. G.; Augustijn-Beckers, P. W. M.; Burt, J. P.; Ware, G. The SCS/ARS/CES Pesticide Properties Database for Environmental Decision-Making. *Rev. Environ. Contam Toxicol.* **1992**, *123*, 1−155.
(50) Diaz-Flores, P. E.; Leyva-Ramos, R.; Rangel-Mendez, J. R.; Ortiz, M. M.; Guerrero-Coronado, R. M.; Mendoza-Barron, J. Adsorption of 2,4-Dichlorophenoxyacetic Acid from Aqueous Solution on Activated Carbon Cloth. *J. Environ. Eng. Manage.* **2006**, *16*, 249−257.
(51) O'Connor, D. J.; Connolly, J. P. The Effect of Concentration of Adsorbing Solids on the Partition Coefficient. *Water Res.* **1980**, *14*, 1517−1523.
(52) Voice, T. C.; Weber, W. J. Sorbent Concentration Effects in Liquid/Solid Partitioning. *Environ. Sci. Technol.* **1985**, *19*, 789−796.
(53) Gschwend, P. M.; Wu, S. On the Constancy of Sediment-Water Partition Coefficients of Hydrophobic Organic Pollutants. *Environ. Sci. Technol.* **1985**, *19*, 90−96.
(54) Zhao, L.-X.; Hou, W.-G. The Effect of Sorbent Concentration on the Partition Coefficient of Pollutants between Aqueous and Particulate Phases. *Colloids Surf., A* **2012**, *396*, 29−34.
(55) Zhao, L.-X.; Song, S.-E.; Du, N.; Hou, W.-G. A Sorbent Concentration-Dependent Langmuir Isotherm. *Acta Phys.-Chim. Sin.* **2012**, *28*, 2905−2910.
(56) Zhao, L.-X.; Song, S.-E.; Du, N.; Hou, W.-G. A Sorbent Concentration-Dependent Freundlich Isotherm. *Colloid Polym. Sci.* **2013**, *291*, 541−550.
(57) Sheindorf, C.; Rebhun, M.; Sheintuch, M. A Freundlich-Type Multicomponent Isotherm. *J. Colloid Interface Sci.* **1981**, *79*, 136−142.
(58) Rao, M. M.; Ramana, D. K.; Seshaiah, K.; Wang, M. C.; Chien, S. W. C. Removal of Some Metal Ions by Activated Carbon Prepared from *Phaseolus aureus* Hulls. *J. Hazard. Mater.* **2009**, *166*, 1006−1013.
(59) Rafatullah, M.; Sulaiman, O.; Hashim, R.; Ahmad, A. Adsorption of Copper(II), Chromium(III), Nickel(II) and Lead(II) Ions from Aqueous Solutions by Meranti Sawdust. *J. Hazard. Mater.* **2009**, *170*, 969−977.
(60) Pehlivan, E.; Altun, T.; Cetin, S.; Iqbal Bhanger, M. Lead Sorption by Waste Biomass of Hazelnut and Almond Shell. *J. Hazard. Mater.* **2009**, *167*, 1203−1208.
(61) González a, M. A.; Pavlovic, I.; Rojas-Delgado, R.; Barriga, C. Removal of Cu^{2+}, Pb^{2+} and Cd^{2+} by Layered Double Hydroxide−Humate Hybrid. Sorbate and Sorbent Comparative Studies. *Chem. Eng. J.* **2014**, *254*, 605−611.
(62) Gui, C.-X.; Wang, Q.-Q.; Hao, S.-M.; Qu, J.; Huang, P.-P.; Cao, C.-Y.; Song, W.-G.; Yu, Z.-Z. Sandwichlike Magnesium Silicate/Reduced Graphene Oxide Nanocomposite for Enhanced Pb^{2+} and Methylene Blue Adsorption. *ACS Appl. Mater. Interfaces* **2014**, *6*, 14653−14659.
(63) Wang, Y.; Wang, G.; Wang, H.; Liang, C.; Cai, W.; Zhang, L. Chemical-Template Synthesis of Micro/Nanoscale Magnesium Silicate Hollow Spheres for Waste-Water Treatment. *Chem.—Eur. J.* **2010**, *16*, 3497−3503.
(64) Lakraimi, M.; Legrouri, A.; Barroug, A.; De Roy, A.; Pierre Besse, J. Preparation of a New Stable Hybrid Material by Chloride-2,4-Dichlorophenoxyacetate Ion Exchange into the Zinc-Aluminium-Chloride Layered Double Hydroxide. *J. Mater. Chem.* **2000**, *10*, 1007−1011.
(65) Dong, C. S.; Li, J. Z.; Sun, Z. X. Synthesis and Transformation of Cerussite and Hydrocerussite. *J. Jinan Univ., Sci. Technol. (Jinan, China)* **2012**, *26*, 73−77.
(66) Crist, B. V. Handbook of the Elements and Native Oxides, Vol. *1*, XPS International, Inc.: Mountain View, CA, 1999.
(67) Liu, Z.; Robinson, J. T.; Sun, X.; Dai, H. PEGylated Nanographene Oxide for Delivery of Water-Insoluble Cancer Drugs. *J. Am. Chem. Soc.* **2008**, *130*, 10876−10877.
(68) Yang, X.; Wang, Y.; Huang, X.; Ma, Y.; Huang, Y.; Yang, R.; Duan, H.; Chen, Y. Multi-Functionalized Graphene Oxide based Anticancer Drug-Carrier with Dual-Targeting Function and pH-Sensitivity. *J. Mater. Chem.* **2011**, *21*, 3448−3454.

DOI: 10.1021/acsami.5b00433
ACS Appl. Mater. Interfaces 2015, 7, 7251−7263